





Electronic stopping power under channeling conditions for slow ions in Ge using first principlesYan-Long Fu ^{1,2} Chang-Kai Li ⁴ Hai-Bo Sang,^{1,2} Wei Cheng ^{1,2,5,*} and Feng-Shou Zhang ^{1,2,3,†}¹*The Key Laboratory of Beam Technology and Material Modification of Ministry of Education, College of Nuclear Science and Technology, Beijing Normal University, Beijing 100875, China*²*Beijing Radiation Center, Beijing 100875, China*³*Center of Theoretical Nuclear Physics, National Laboratory of Heavy Ion Accelerator of Lanzhou, Lanzhou 730000, China*⁴*The Institute of Technological Science, Wuhan University, Wuhan 430072, China*⁵*Ningbo Institute of Industrial Technology, Chinese Academy of Sciences, Ningbo, Zhejiang 315201, China*

(Received 7 January 2020; revised 12 May 2020; accepted 16 June 2020; published 7 July 2020)

The electronic stopping power for low-velocity ions (including protons and α particles) in the semiconductor Ge is investigated with the aid of time-dependent density functional theory based on Ehrenfest dynamics. The purpose of this study is to further learn about the energy loss mechanisms of the slow ions. When the projectile ions pass through the crystal film along the $\langle 100 \rangle$, $\langle 110 \rangle$, and $\langle 111 \rangle$ channels, we analyze the channeling effect of the electronic stopping power in detail by investigating the channeling electronic density, the stopping force, and the trapped electrons. Our results are in good agreement with the available experimental data and the other theoretical calculations, which demonstrate that this approach is able to reasonably describe the electronic stopping power. Furthermore, these results can act as the reference data for the ion-beam irradiation of Ge in the low-energy regime.

DOI: [10.1103/PhysRevA.102.012803](https://doi.org/10.1103/PhysRevA.102.012803)**I. INTRODUCTION**

The energy deposited in ion irradiation is of great interest in a wide range of research fields, such as medicine (e.g., ion-beam therapy for cancer) [1], nuclear safety (e.g., irradiance resistance of materials in nuclear reactors) [2], space exploration [3], and nanotechnology (e.g., material modification) [4].

When an energetic ion travels through the material, it is decelerated due to the interaction with the electrons and nuclei of the medium; the first force is known as the electronic stopping power (S_e), the second force is known as the nuclear stopping power (S_n). The stopping power (SP) describes the magnitude of energy loss per unit length for the projectile ion, i.e.,

$$S = dE/dx = Qv, \quad (1)$$

where Q is the value of the friction coefficient. For the S_e , it is proportional to the ion velocity [5,6] and describes the rate of energy transfer from the projectile ion to the electrons of the medium.

In the experiment, the high-purity Ge detector is a kind of nuclear radiation detector made of Ge crystal [7,8]. For the application of semiconductor detector in the irradiation environment, the S_e is a key physical quantity to investigate and identify radiation sources. Additionally, it is known that the channelling phenomenon is widely used in the implantation technology of the semiconductor device [9,10], in which the S_e also plays a crucial role in irradiation damage of the materials.

At ionic velocities v below the Fermi velocity v_F , the projectile ions interact only with weakly bound electrons in the conduction or valence band of the medium system. In addition, when the light projectile ion moves along a channeling trajectory in the medium, it does not directly interact with the host atoms, but interacts with the electrons around the host atoms. In this process, the S_e of the projectile ions has a strong dependence on the projectile velocity (i.e., the ion energy). Since the energy loss process of the projectile ion is dominated by the electronic excitation and ionization of the medium, the captured electron must be taken into account in this process. Indeed, in particular for the light ions, e.g., proton (H^+ ion) and α particle (He^{2+} ion), the proportionality of the electronic stopping power to the velocity is stronger at slow velocities for most targets [11–14].

For the S_e in the metals and insulators, in the range of slow velocities, there are more extensive research results [15–26]; however, for the semiconductor materials with the electronic band structure between metal and insulator, there is a lack of more extensive investigation on the S_e of semiconductors [27,28]. Although the electronic band structure of the semiconductor also has a band gap, the band gap is much smaller than that of insulators. Because the electronic band structure of semiconductor has a narrow band gap, it has the special conductivity; only when the electrons of the valence band are excited and pass through the band gap can the semiconductor be conductive, and this results in the electronic energy loss. Therefore, it is very meaningful to study the influence of the electronic band structure on the electronic stopping power of semiconductors.

In experiments, for the projectile ion at low energies, the S_e is deduced by using time-of-flight low-energy ion scattering (TOF-LEIS) spectrometer [12,14,22,29–33] measurements.

*Corresponding author: chengwei@bnu.edu.cn†Corresponding author: fszhang@bnu.edu.cn

For the theoretical investigation of S_e , the time-dependent density functional theory (TDDFT) method [34] is generally employed to simulate the interaction between the slow projectile ion and the target atoms, where the interacting electrons are assumed to be a homogenous electron gas (HEG). Based on the HEG model, Fermi and Teller [35] found and pointed out that the S_e exhibited velocity proportionality for $v < 1$ a.u. (atomic units with $|e| = m = \hbar = 1$ herefore), which was verified in many experiments on metal materials. For the target materials with the band gap (e.g., insulators and semiconductors), the excitation of electron-hole pairs requires a minimum excitation energy E_{\min} (i.e., the threshold value) [36–38] because the excited electrons in the valence band need to pass through the band gap; in this process, the required energy comes from the kinetic energy of the projectile ion. Below this minimum excitation energy, the energy dissipation would be suppressed, which leads to a threshold effect of S_e with respect to the projectile velocity. That is to say, below this threshold velocity, the S_e would be strictly zero (i.e., vanishing electronic stopping power). Previous experimental and theoretical investigations reveal that there is a threshold velocity for a light projectile ion (e.g., a proton or an α particle) passing through an insulator with large band gap (e.g., LiF, KCl, SiO₂, and HfO₂) [13,26,32,39]. Recently, experimental research [29] reported that the semiconductor Ge with the band gap of 0.67 eV (at room temperature) exhibited a clear threshold velocity in the range of slow velocities.

In this paper, we investigate the S_e of H⁺ and He²⁺ ions in Ge under channeling conditions for energies below 27 keV/u (i.e., ionic velocities $v < 1$ a.u.) by using TDDFT simulations. The results are compared to the experimental S_e by Roth *et al.* [29] and with the calculated S_e by Ullah *et al.* [40], as well as with the SRIM-2013 [41,42] simulations. The S_e under channeling conditions presents the directional dependence and displays a strong quantitative difference for H⁺ and He²⁺ ions, which are closely related to the stopping force and the electronic exchange between the projectile ions and the medium atoms; this electronic exchange mechanism is regarded as a way different from direct electron-hole pair excitation. Therefore, we explore how the electronic exchange affects the S_e .

The remainder of the paper is as follows. In Sec. II, we briefly introduce the established crystal model and the calculation method. In Sec. III, the results and discussions we present mainly include the following several components. In the first part, we discuss the influence of the channeling effect and the electron transfer on the electronic energy dissipation in the collisions; and the friction coefficient in different channels is explored. In the second one, we investigate the S_e of different impact parameters. In Sec. IV, we outline the main conclusions and results.

II. CALCULATION METHODS AND CRYSTAL STRUCTURES

In this work, the Ehrenfest dynamics time-dependent density functional theory (ED-TDDFT) [43–48] based on the OCTOPUS code package is employed to simulate the collision dynamic process between the projectile and the electrons of the medium system. This model is known as a semiclassical

molecular dynamics (MD) model, the nucleus is treated as a classical system and coupled with the quantum electron system outside the nucleus, which has frequently been used and tested in many systems [13,39,49,50]. The specific methodology is described in detail in Refs. [48,50–53]. As the projectile ion moves, the TDKS equation is employed to describe the evolution of the electronic density with time and the total energy of the system.

TDDFT is built in the form of time-dependent Kohn-Sham (TDKS) equation for the orbital ψ_i of an effective single electron. These states obey a self-consistent Schrödinger-like Kohn-Sham equation, as follows:

$$i\hbar \frac{\partial}{\partial t} \psi_i(\vec{r}, t) = \left(-\frac{\hbar^2}{2m} \nabla^2 + V_{\text{KS}}[n](\vec{r}, t) \right) \psi_i(\vec{r}, t), \quad (2)$$

where \vec{r} and t are the spatial and time coordinates, respectively. At time t , the instantaneous electronic density is

$$n(\vec{r}, t) = \sum_i |\psi_i(\vec{r}, t)|^2, \quad (3)$$

which is given by the sum of single-electron probabilities. The KS effective potential V_{KS} is written as

$$V_{\text{KS}}[n](\vec{r}, t) = V_{\text{ext}}[R(t), \vec{r}] + V_H[n](\vec{r}, t) + V_{\text{XC}}[n](\vec{r}, t), \quad (4)$$

where the first term $V_{\text{ext}}[R(t), \vec{r}]$ denotes the external potential (i.e., the interaction of the ions with the electrons), thence $R(t)$ is the ionic position of time t ; the second term $V_H[n](\vec{r}, t)$ denotes the Hartree potential (i.e., the classical electron-electron interaction); the last term $V_{\text{XC}}[n](\vec{r}, t)$ is the exchange-correlation (XC) potential. In this work, the Perdew-Wang local density approximation (PW-LDA) [54] is employed as an adiabatic time-dependent XC functional, more detailed description about time-dependent XC functional is described in Refs. [55,56].

Ionic coordinates follow Newton's equations $M_I \ddot{R}_I(t) = F_I$. The forces F_I are Ehrenfest forces, which are derived from the assumptions of the classical behavior of ions. All of the above together, this set of equations is the so-called ED-TDDFT dynamics.

The S_e is extracted from the energy deposited in the electronic system, i.e., the energy deposited per unit length $S_e(x) = dE(x)/dx$; the projectile position x changes as a function of the time t . The time-dependent energy $E(t)$ is given by

$$E(t) = \sum_i \int d\vec{r} \psi_i^*(\vec{r}, t) \left(-\frac{\hbar^2}{2m} \nabla^2 + V_{\text{ext}}(\vec{r}) \right) \psi_i(\vec{r}, t) + E_{\text{HXC}}[n] + E_{\text{ion-ion}}[R_I(t)] + \frac{1}{2} \sum_I M_I \dot{R}_I^2(t). \quad (5)$$

Here, the equation consists of the electronic kinetic energy, the ion-electron potential energy (external), the Hartree and exchange-correlation (HXC) of the electron-electron interaction, the configurational energy $E_{\text{ion-ion}}[R_I(t)]$, and the ionic kinetic energy.

In this model, the forces and potential energy applied to the ions are evolved “on the fly” as the simulation proceeds. In ED-TDDFT, the included transitions between electronic

adiabatic states couple it with the populations of the adiabatic states to the nuclei trajectories [47]. The excited electronic states are calculated by means of the *ab initio* molecular dynamics (AIMD) simulation, which provides a way to investigate the electronic transfer between the projectile ion and the medium atoms in the collisions. In the present work, we mainly focus on the light ions in the range of low velocities in which the core electrons are frozen, only the weakly bound valence electrons are involved in the interaction; in this case, the norm-conserving Troullier-Martins pseudopotential [57] is used to describe the coupling of valence electrons to ionic cores. In this ED-TDDFT simulation, the approximate *enforced time-reversal symmetry* (ETRS) method [58] is used to propagate the electronic wave functions, and the velocity Verlet algorithm is embedded in the ionic motion equations, which provide an orthogonalization free AIMD calculation that it is able to enhance computational efficiency.

The system we investigate is a $2 \times 2 \times 2$ supercell structure comprising 64 Ge atoms with the *FD-3M* (No. 227) symmetrical space group. The chosen lattice parameter is 11.315 Å, which is twice the length of the experimentally reported value of 5.6575 Å in Ref. [59]. For this reason, on the premise of controlling the cost and computational complexity, the above-mentioned supercell is selected to minimize the impact of the crystalline size on the study. We put the supercell in the center of a parallelepiped box as a simulation unit, in which the total size of the simulation box is large enough to minimize the interference caused by the boundary, and to achieve an environment similar to that of the experiment. In the simulation box, the electronic density, KS orbitals, and external potential are discretized on a set of grid points; the uniform space between the grid points is 0.16 Å. The propagation of the projectile is carried out using a time step of 0.001 fs, which avoid the instability of the calculation results and ensured the stability of the numerical integration.

At first, to obtain the unperturbed electronic density distribution of the crystal Ge (i.e., the ground state of the bulk medium, and the projectile particle at its initial position), we put the projectile ion outside the simulation box. The results of the convergent ground state (with the projectile ions not included) are obtained by the calculation of the initial crystal structure using density functional theory. This state is now being regarded as the initial conditions of the projectile passing through the medium material with some finite velocity. Afterwards, the next natural step is that the H^+ ion or the He^{2+} ion moves rectilinearly and with a constant velocity passing through the test medium [17,45,60–62]. Therefore, the crystals with various orientations are modified with the proton and α particle, to which all atoms are fixed (semiconductor, Ge) in thermodynamic equilibrium positions. This approximation is due to the fact that the effect of background Ge atoms' movement on the system at low temperatures is negligible compared to an ion passing at the attosecond level [17,45,60–62]. The projectile penetrates the different channels of the background material [63] along the negative direction of the z axis, and thus, there is no direct interaction between the projectile ion and the target nucleus, but the ion indirectly interacts with the electrons around the medium atoms. It should be noted that, although the nucleus remains stationary, the electronic density distribution varies with the time.

III. RESULTS AND DISCUSSION

A. Channeling effect of S_e

In the following, we systematically investigate the S_e of H^+ and He^{2+} ions in the semiconductor Ge under channeling conditions; the values in a velocity regime of 0.1–1.0 a.u., obtained from TDDFT simulation, are depicted in Fig. 1. To compare the present results, the values predicted by the SRIM-2013 [41,42], together with the experimental S_e by Roth *et al.* [29] and the calculated S_e by Ullah *et al.* [40] based on the SIESTA program, are presented in Fig. 1. As we can see, a striking phenomenon is the direction dependence of the S_e . Additionally, in the range of slow velocities, the calculated S_e for the H^+ and He^{2+} ions are directly proportional to the projectile velocity in the channels, and our calculated S_e is in good agreement with the experimental data [29].

For the S_e in the $\langle 100 \rangle$ and $\langle 111 \rangle$ channels, our data exhibit minor deviations from the SRIM-2013 curve, which is due to the fact that the SRIM results are semi-empirical by averaging a large number of different impact parameters in various incident directions. For H^+ ion in the $\langle 100 \rangle$ and $\langle 111 \rangle$ channels, our results agree reasonably well with the experimental data for velocities below 0.45 a.u. At higher velocities up to 0.6 a.u., the experimental data exceed the simulated values by about 20%, which may be due to that fact that it is impossible to apply the same conditions as the experimental operation to simulate all kinds of random projectile trajectories on diverse parts of the supercell. In contrast to the H^+ ion, the more complex projectile He^{2+} presents much stronger S_e in the same conditions, which is attributed to the fact that the electron-hole pairs excitation is more efficient in the He^{2+} case due to the stronger interactions between ion and electrons. For all investigated velocities, the S_e of H^+ and He^{2+} ions in the $\langle 100 \rangle$ and $\langle 111 \rangle$ channels are greater than that of $\langle 110 \rangle$ channel, as shown in Figs. 1(a) and 1(b). For the He^{2+} ion, the S_e of the $\langle 100 \rangle$ and $\langle 111 \rangle$ channels yield very good agreement with the SRIM simulations, similarly as for the H^+ ion. This comparison allows us to investigate whether the channeling electron density and the stopping force as well as the electron transfer have an influence on the S_e of different channels.

Therefore, in the following subsections, we discuss the impact of these quantities on the channeling S_e .

1. Electronic density and stopping force in the channel

Figure 2 presents the channeling electronic density in the ground state. The way of calculating this physical quantity is to integrate the electronic density in a small cylinder with a radius of $r = 0.32$ Å along the axial channel, and the total number of electrons for each step is sequentially obtained, divided by the volume of the corresponding cylinder step-by-step. If the integration radius gets larger, it may include more free electrons (inner electrons) of the host atoms that are not disturbed by the intruding ion; however, if the radius is too small, the partially disturbed electrons may not be taken into account, so the channeling electron density cannot be accurately presented.

As shown in Fig. 2, the electronic density presents the cyclic fluctuation, which indicates the periodicity of the

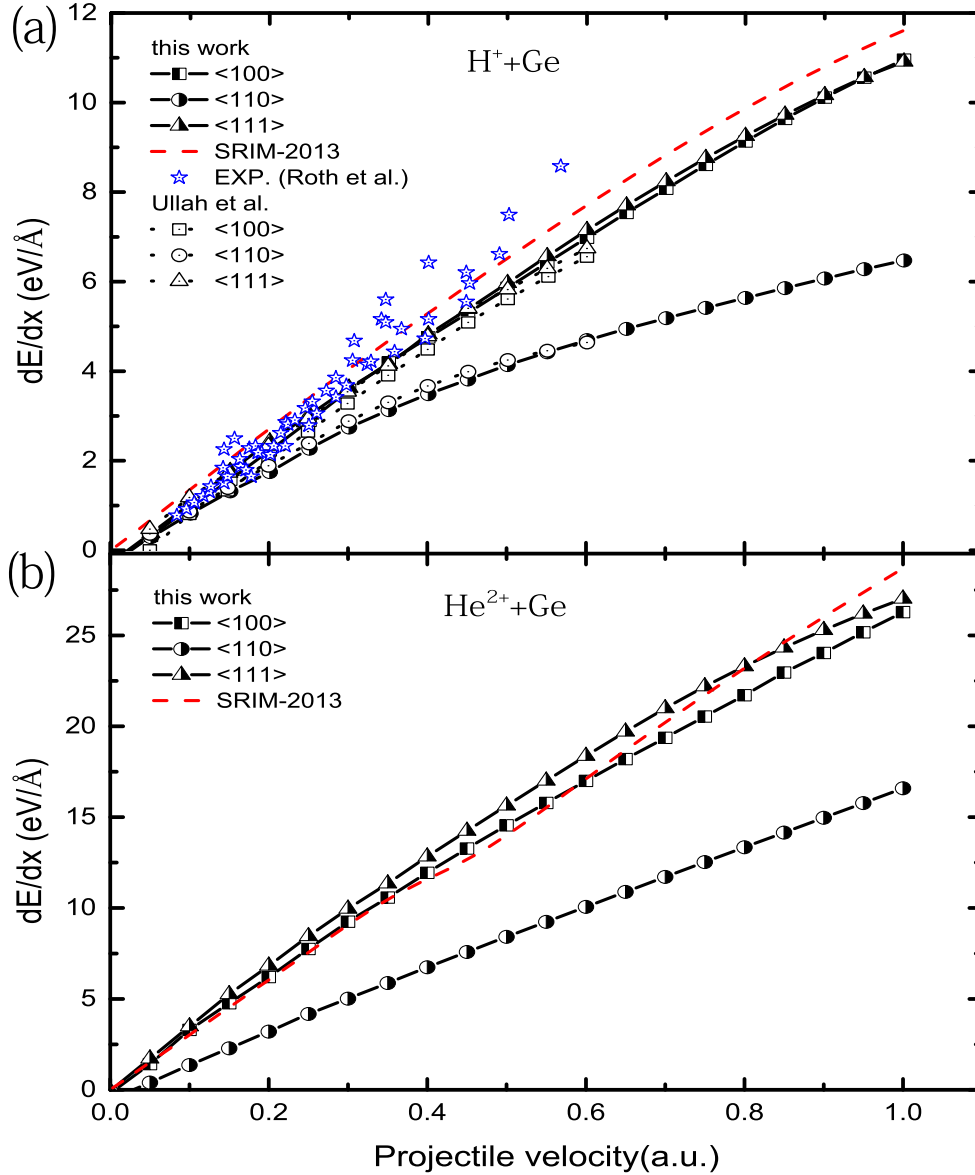


FIG. 1. Electronic stopping power of (a) H^+ and (b) He^{2+} ions in the crystal Ge along the $\langle 100 \rangle$, $\langle 110 \rangle$, and $\langle 111 \rangle$ channels. The data obtained in this work are compared to previously experimental data [29] and theoretical calculations [40] from the SIESTA program.

atomic arrangement in the crystal. In addition, the trend of the $\langle 111 \rangle$ curve shows that its amplitude is significantly larger than that of the other two channels. To quantitatively compare the density, with the help of dividing the total number of electrons in the channel by the volume of whole cylinder, the average electronic concentration obtained in the $\langle 100 \rangle$, $\langle 110 \rangle$, and $\langle 111 \rangle$ channels are 0.1356, 0.0291, and 0.1742 electrons $\cdot \text{\AA}^{-3}$, respectively. We find that, although the amplitude of $\langle 100 \rangle$ channel is small, the average effect displays the almost same electronic concentration in the $\langle 100 \rangle$ and $\langle 111 \rangle$ channels, and the electronic distribution of the $\langle 110 \rangle$ channel is most dilute; in a low electronic density channel, the electronic energy loss is less because the electron-hole pairs' excitation is weak, so it leads to a small S_e . These behaviors are consistent with the channeling S_e in Fig. 1. Therefore, the data indicate that the direction dependence of S_e is related to the electronic density in the channel, which strongly expounds

and verifies the suppositions of the earlier research in the literature [40,64,65].

Furthermore, we investigate the stopping force (i.e., the radial force in the Refs. [17,60]) acting on the projectile ion with a velocity of 0.5 a.u. along the channels; the results for H^+ and He^{2+} ions are depicted in Figs. 3(a) and 3(b), respectively. It is worth noting that the radial force oscillates as the projectile ion moves along the channel. The magnitude of the stopping force implies the intensity of Coulomb interaction between the projectile ion and the atoms around the corresponding trajectory. Compared to the H^+ ion in Fig. 3(a), the stopping force of the He^{2+} ion depicted in Fig. 3(b) is stronger. This result coincides with the S_e in Figs. 1(a) and 1(b), i.e., in the same channel, the S_e of the He^{2+} ion is significantly greater than that of the H^+ ion; the increased stopping force exerted by the medium on the projectile ion can lead to greater energy loss (i.e., the higher S_e). Additionally,

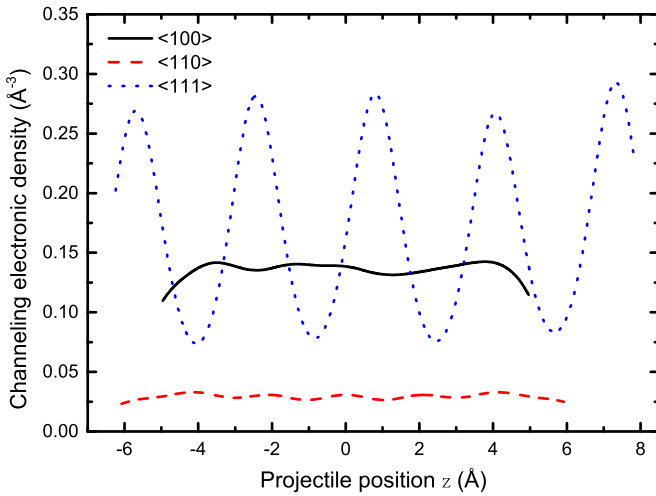


FIG. 2. Electronic density as a function of the projectile position z in the $\langle 100 \rangle$ (black solid line), $\langle 110 \rangle$ (red dashed line), and $\langle 111 \rangle$ channels (blue dotted line).

we find that the trend of the stopping force is similar to that of the corresponding electronic density, which potentially suggests that a proportional coefficient exists between them.

2. Electron transfer effect in the channel

The periodic charge-exchange is regarded as a mechanism which dominates the electronic energy loss in the literature

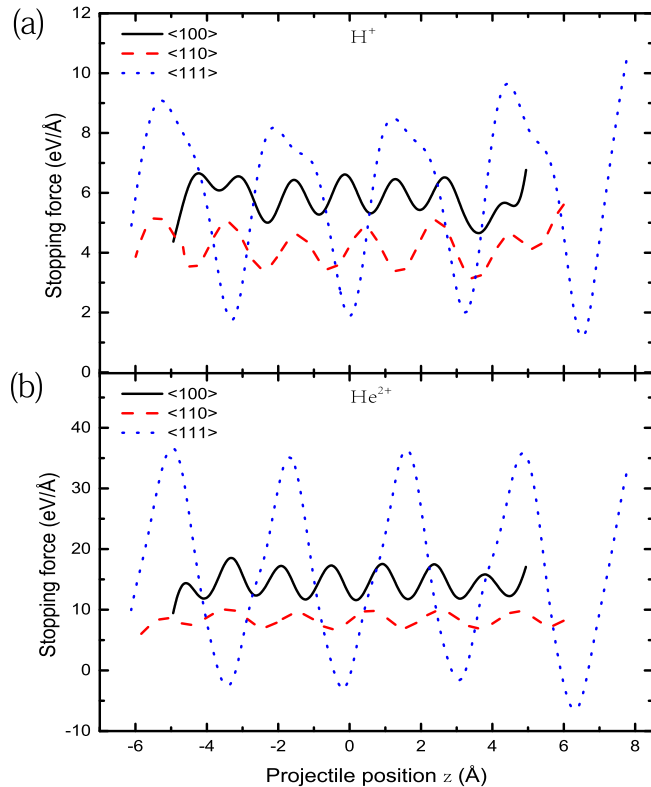


FIG. 3. Stopping force exerted on the (a) H^+ and (b) He^{2+} ions when the projectile ion with a velocity of 0.5 a.u. pass through the medium Ge along three different channels.

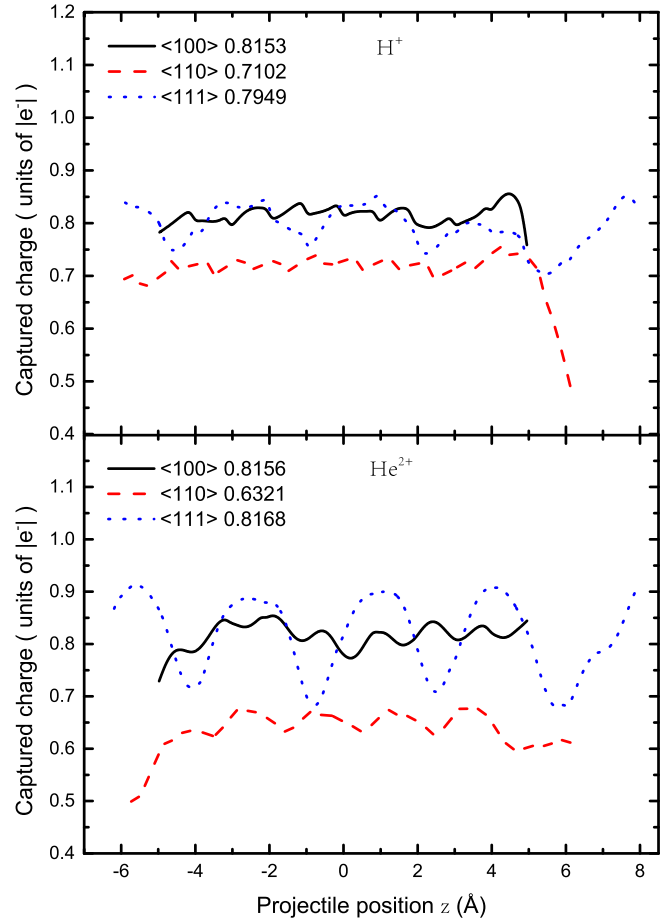


FIG. 4. The captured charge of the (a) H^+ and (b) He^{2+} ions with a velocity of 0.5 a.u. along three different channeling trajectories. The average captured electrons for the H^+ in the whole $\langle 100 \rangle$, $\langle 110 \rangle$, and $\langle 111 \rangle$ channels are 0.8153, 0.7102, and 0.7949 units of $|e^-|$, respectively. The corresponding values for the He^{2+} ion are 0.8156, 0.6321, and 0.8168 units of $|e^-|$.

[12,24,26,29,31,66], but there is a lack of quantitative presentation and investigation in detail. For this reason, the impact of the charge-exchange on the channeling S_e is investigated; in Figs. 4(a) and 4(b), we present the electron transfer of H^+ and He^{2+} ions with a velocity of 0.5 a.u. moving along the $\langle 100 \rangle$, $\langle 110 \rangle$, and $\langle 111 \rangle$ channels. The number of electrons captured by the projectile ion is extracted by quantitatively integrating the valence electronic density in the spherical volume with a radius of $r = 1.28 \text{ \AA}$ around the projectile ion and subtracting the number of electrons of the ground state within the corresponding spherical volume.

It can be seen from Fig. 4 that the charge-exchanges in the $\langle 100 \rangle$ and $\langle 110 \rangle$ channels are small amplitude and high frequency, which is associated with the distribution of the channeling electronic density (see Fig. 2). Although the charge-exchange of the projectile along the $\langle 100 \rangle$ channel is small amplitude, the average captured electron in the $\langle 100 \rangle$ channel is very close to that of the projectile in the $\langle 111 \rangle$ channel. In addition, we find that the average captured electrons of the projectile in the $\langle 100 \rangle$ and $\langle 111 \rangle$ channels are larger than that of the projectile in the $\langle 110 \rangle$ channel, which implies more

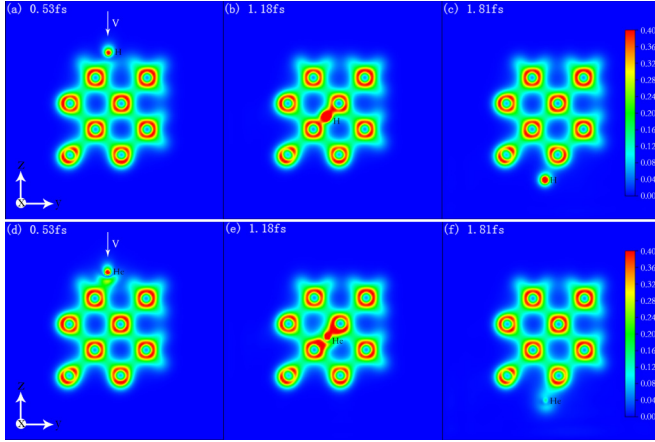


FIG. 5. Time evolution of the electronic density for (a)–(c) H^+ and (d)–(f) He^{2+} ions passing the medium Ge along the $\langle 100 \rangle$ channel with the velocity of 0.5 a.u. Note that the density distribution is plotted in the $x = x_{\text{ion}}$ (x_{ion} , i.e., the x coordinate value of the projectile ion) scattering plane.

charge-exchanges in the $\langle 100 \rangle$ and $\langle 111 \rangle$ channels. Therefore, this feature lead to the fact that the S_e of the projectile along the $\langle 100 \rangle$ and $\langle 111 \rangle$ channels is higher than that of the projectile along the $\langle 110 \rangle$ channel (as shown in Fig. 1).

In Fig. 4, we find the irregular captured electron behavior of the projectile ion around $z = \pm 5$, which results from the asymmetric arrangement of the atoms at the border of the crystal and the nonequilibrium process between neutralization and reionization of the projectile ion. Another reason for this irregular behavior is the abnormal electron-exchange between the projectile ion and the target crystal because of the irregular electronic density distribution at the border of the crystal (as shown in Fig. 2).

Under the same channeling conditions, an interesting phenomenon we find is that the electronic exchange frequency of H^+ is faster than that of He^{2+} , i.e., an active charge-exchange with the H^+ ion. This behavior is due to the fact that only one electron at the H-1s level is easier to perturb the electronic system and exchange electrons with the atoms near the channel. However, from another point of view, we find that the averaging captured charge of the He^{2+} ion is slightly greater than that of the H^+ ion in the channel, which is attributed to the fact that the H-1s level (i.e., being occupied by two electrons) can increase the probability of the electronic exchange between the projectile and the medium atoms. Therefore, for the He^{2+} ion, the more captured electrons lead to the increased energy loss, i.e., the larger S_e ; this result corresponds well with the S_e in Fig. 1. The periodic electron exchange serves as a driving force for the internal excitation of the projectile, which is different from the direct excitation of electron-hole pairs in the interactions of ions with electrons.

To more intuitively present the electron transfer, the evolution of the electronic density with time when the H^+ and He^{2+} ions of $v = 0.5$ a.u. travels through the medium Ge along the $\langle 100 \rangle$ channel are shown in Fig. 5. We find that the electronic exchange is a local perturbation process [62,67]. At the beginning, the incident ion is a fully bare projectile. When the projectile ions come closer to the medium, at $t = 0.53$ fs,

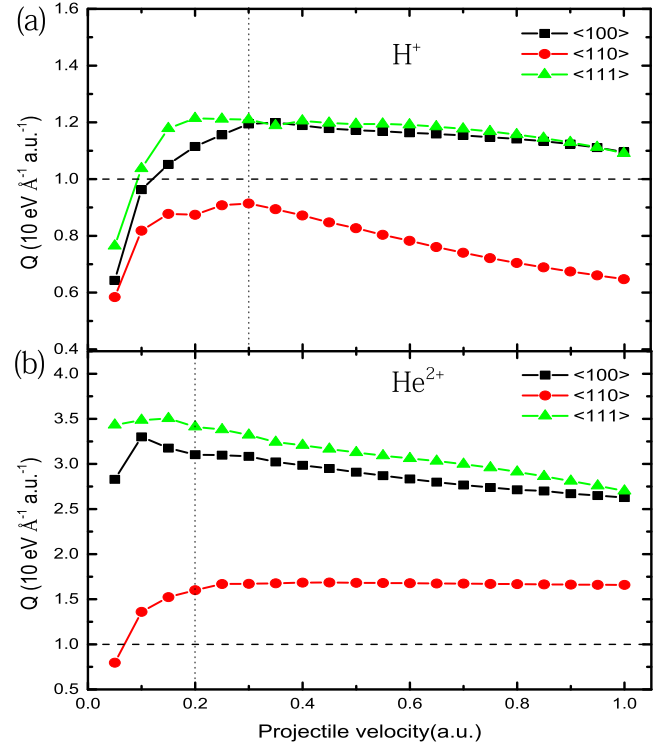


FIG. 6. Friction coefficient Q for the (a) H^+ and (b) He^{2+} ions in Ge as a function of the projectile velocity in the $\langle 100 \rangle$, $\langle 110 \rangle$, and $\langle 111 \rangle$ channels.

the projectile ions indirectly encounter the medium atoms at close range (i.e., where the projectile ions interact with the electrons of the system.), and capture a small amount of electrons. At $t = 1.18$ fs [see Figs. 5(b) and 5(e)], the projectile ions are encapsulated by a large number of electrons resulting from the electronic exchange with the medium atoms; at this moment, the electronic clouds and chemical bonds are formed around the projectiles. In the semiconductor Si, similar transition bonds were observed [68]. Eventually, at $t = 1.81$ fs, the projectile ions leave the simulation unit and the ions carry a portion of electrons from the medium Ge. Furthermore, compared to the induced ion H^+ [see Fig. 5(b)], an obvious phenomenon is that the He^{2+} ion [see Fig. 5(e)] is able to perturb a larger region of electron distribution.

3. Friction coefficient at different velocities in the channel

In Fig. 6, we present the friction coefficient Q of H^+ and He^{2+} with different ion velocity in the channeling directions. For the H^+ ion in all three channels, in Fig. 6(a), the friction coefficients are observed to be inversely proportional to projectile velocities for v down to 0.3 a.u., i.e., the Q increases monotonously with the decreasing velocity. In the case of the He^{2+} ion in the $\langle 100 \rangle$ and $\langle 111 \rangle$ channels, the results shown in Fig. 6(b) have the same trend as for H^+ in Fig. 6(a) for v down to 0.2 a.u.; while an interesting phenomenon is that the Q is almost constant (about $16 \text{ eV } \text{\AA}^{-1} \text{ a.u.}^{-1}$) for the $\langle 110 \rangle$ channel, a possible explanation is due to the electronic density in this channel is extremely dilute (see Fig. 2). For the H^+ at $v < 0.3$ a.u. and the He^{2+} at $v < 0.2$ a.u., the decreasing Q

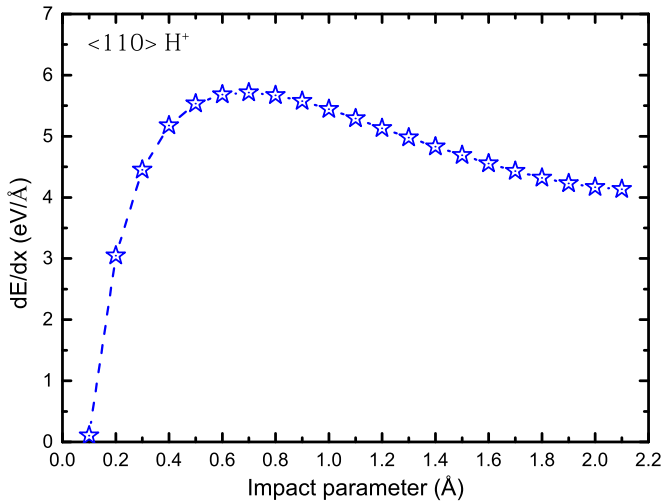


FIG. 7. The S_e as a function of the impact parameter for the projectile H^+ with a velocity of 0.5 a.u. passing the bulk Ge along the $\langle 110 \rangle$ channel of different impact parameter.

value may be due to the fact that the change of the number of available electrons excited by the projectile ion in this velocity region; it is also possible that the time of the projectile stay in the channel is too long and results in a drop of Q value.

B. Influence of impact parameter on the S_e

To unveil the influence of the impact parameter on the S_e [69], as shown in Fig. 7, we investigate the S_e of the 0.5 a.u.- H^+ ion traveling through the Ge film along the $\langle 110 \rangle$ channel in the range of the impact parameter from 0.1 to 2.1 Å (i.e., the max impact parameter, the channel center). Here, the impact parameter value is defined as the closest distance between the projectile ion's trajectory and the nearby Ge atom; the trajectory along the central axis of the channel has the largest impact parameter, and the trajectory closest to the Ge atoms has the smallest impact parameter.

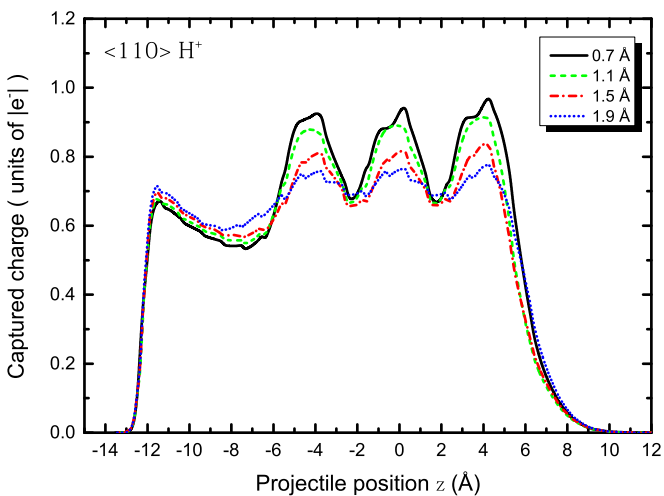


FIG. 8. The captured charge for the projectile H^+ with a velocity of 0.5 a.u. passing the bulk Ge along the $\langle 110 \rangle$ channel of different impact parameter (including 0.7, 1.1, 1.5, and 1.9 Å).

The results show that, in the case of an impact parameter of 0.7 Å, the S_e reaches the maximum 5.72 eV/Å; we find that this value is in better accordance with the SRIM and the experimental data in Fig. 1. With the increase of impact parameters, the S_e gradually decline and reach a platform. This trend is attributed to the fact that the larger impact parameters lead to the fewer electrons excited and transferred from the medium atoms to the projectile H^+ , so the less energy dissipation of electrons.

To demonstrate the relationship between the impact parameter and the captured charge, we investigate the electron transfer of the H^+ ion in the $\langle 110 \rangle$ channel for the impact parameters of 0.7, 1.1, 1.5, and 1.9 Å, adopting the same integral method as in Fig. 4; the results are shown in Fig. 8. As can be seen, the amplitude of the electron transfer of 0.7 Å is obviously larger than that of the other impact parameters. With the increase of the impact parameter value, the amplitude of the electron transfer gradually declines, implying the reduced energy loss (i.e., the smaller electronic stopping power). This trend coincides with that of the S_e as a function of the impact parameter. Therefore, once again demonstrating that the electron transfer is a way of attributing S_e .

IV. CONCLUSION

In this work, the S_e of the H^+ and He^{2+} ions in the semiconductor Ge along the $\langle 100 \rangle$, $\langle 110 \rangle$, and $\langle 111 \rangle$ channels are investigated by means of ED-TDDFT simulations. Our results predicted from theory are satisfactory compared to the existing experimental data [29] and theoretical calculations [40]. The S_e for the H^+ and He^{2+} ions exhibit a linear velocity proportionality in the range of slow velocities (0.1–1.0 a.u.).

Additionally, the channeling effect of S_e is analyzed by calculating the channeling electronic density, the stopping force, and the captured charge. We find that there is a proportional coefficient between the channeling electronic density and the stopping force. By analyzing the captured charge under channeling conditions, a remarkable phenomenon we find is that the values of the $\langle 100 \rangle$ and $\langle 111 \rangle$ channels begins to be larger than that of the $\langle 110 \rangle$ channel, which is in agreement with the trend of the S_e in the channels. This trend implies that the resulting S_e is mainly determined by the electronic transfer between the projectile ion and the medium atoms in the collisions. On the other hand, we investigate the dependence of the S_e on the impact parameter and evaluate the captured charge of different impact parameter for the H^+ in bulk Ge along the $\langle 110 \rangle$ channel. While the impact parameter is 0.7 Å, the S_e reaches the maximum 5.72 eV/Å, which helps to better compare to the SRIM value and the experimental data [29].

ACKNOWLEDGMENTS

This work was supported by the National Natural Science Foundation of China under Grants No. 11635003, No. 11025524, and No. 11161130520; the National Basic Research Program of China under Grant No. 2010CB832903; and the European Commissions Seventh Framework Program (FP7-PEOPLE-2010-IRSES) under Grant Agreement Project No. 269131.

- [1] A. V. Solov'yov, E. Surdutovich, E. Scifoni, I. Mishustin, and W. Greiner, *Phys. Rev. E* **79**, 011909 (2009).
- [2] F. Komarov, A. Komarov, V. V. Pilko, and V. Pilko, *J. Eng. Thermophys.* **86**, 1481 (2013).
- [3] O. Ilic, C. M. Went, and H. A. Atwater, *Nano Lett.* **18**, 5583 (2018).
- [4] S. Kim, S. Lee, and J. Hong, *ACS Nano* **8**, 4698 (2014).
- [5] J. E. Valdés, J. C. Eckardt, G. H. Lantschner, and N. R. Arista, *Phys. Rev. A* **49**, 1083 (1994).
- [6] I. Nagy and B. Apagyi, *Phys. Rev. A* **58**, R1653(R) (1998).
- [7] J. Hansen, J. McGeorge, D. Nix, W. Schmidt-Ott, I. Unus, and R. Fink, *Nucl. Instrum. Methods* **106**, 365 (1973).
- [8] J. Bruckner, M. Korfer, H. Wanke, A. Schroeder, D. Filges, P. Dragovitsch, P. Englert, R. Starr, J. Trombka, I. Taylor, D. M. Drake, and E. R. Shunk, *IEEE Trans. Nucl. Sci.* **38**, 209 (1991).
- [9] E. Rimini, *Ion Implantation: Basics to Device Fabrication*, Vol. 293, (Springer Science & Business Media, New York, 1994).
- [10] K. Tsukamoto, T. Kuroi, and Y. Kawasaki, in *Ion Implantation Technology 2101: 18th International Conference on Ion Implantation Technology IIT 2010*, edited by J. Matsuo, M. Kase, T. Aoki, and T. Seki, AIP Conf. Proc. No. 1321, (AIP, College Park, MD, 2011), pp. 9–16.
- [11] G. Martínez-Tamayo, J. C. Eckardt, G. H. Lantschner, and N. R. Arista, *Phys. Rev. A* **54**, 3131 (1996).
- [12] D. Goebel, D. Roth, and P. Bauer, *Phys. Rev. A* **87**, 062903 (2013).
- [13] C.-K. Li, F. Wang, B. Liao, X.-P. OuYang, and F.-S. Zhang, *Phys. Rev. B* **96**, 094301 (2017).
- [14] D. Roth, B. Bruckner, G. Undeutsch, V. Paneta, A. I. Mardare, C. L. McGahan, M. Dosmailov, J. I. Juaristi, M. Alducin, J. D. Pedarnig, R. F. Haglund, Jr., D. Primetzhofer, and P. Bauer, *Phys. Rev. Lett.* **119**, 163401 (2017).
- [15] J. Valdés, G. aMartínez Tamayo, G. Lantschner, J. Eckardt, and N. Arista, *Nucl. Instrum. Methods Phys. Res., Sect. B* **73**, 313 (1993).
- [16] P. Riccardi, R. A. Baragiola, and C. A. Dukes, *Phys. Rev. B* **92**, 045425 (2015).
- [17] E. E. Quashie, B. C. Saha, and A. A. Correa, *Phys. Rev. B* **94**, 155403 (2016).
- [18] M. A. Zeb, J. Kohanoff, D. Sánchez-Portal, A. Arnau, J. I. Juaristi, and E. Artacho, *Phys. Rev. Lett.* **108**, 225504 (2012).
- [19] S. N. Markin, D. Primetzhofer, S. Prusa, M. Brunmayr, G. Kowarik, F. Aumayr, and P. Bauer, *Phys. Rev. B* **78**, 195122 (2008).
- [20] C. Celedón, E. A. Sánchez, M. S. Moreno, N. R. Arista, J. D. Uribe, M. Mery, J. E. Valdés, and P. Vargas, *Phys. Rev. A* **88**, 012903 (2013).
- [21] D. Roth, C. Celedon, D. Goebel, E. Sanchez, B. Bruckner, R. Steinberger, J. Guimpel, N. Arista, and P. Bauer, *Nucl. Instrum. Methods Phys. Res., Sect. B* **437**, 1 (2018).
- [22] D. Roth, B. Bruckner, M. V. Moro, S. Gruber, D. Goebel, J. I. Juaristi, M. Alducin, R. Steinberger, J. Duchoslav, D. Primetzhofer, and P. Bauer, *Phys. Rev. Lett.* **118**, 103401 (2017).
- [23] J. I. Juaristi, C. Auth, H. Winter, A. Arnau, K. Eder, D. Semrad, F. Aumayr, P. Bauer, and P. M. Echenique, *Phys. Rev. Lett.* **84**, 2124 (2000).
- [24] C. Auth, A. Mertens, H. Winter, and A. Borisov, *Phys. Rev. Lett.* **81**, 4831 (1998).
- [25] E. Artacho, *J. Phys.: Condens. Matter* **19**, 275211 (2007).
- [26] J. M. Pruneda, D. Sánchez-Portal, A. Arnau, J. I. Juaristi, and E. Artacho, *Phys. Rev. Lett.* **99**, 235501 (2007).
- [27] A. Lim, W. M. C. Foulkes, A. P. Horsfield, D. R. Mason, A. Schleife, E. W. Draeger, and A. A. Correa, *Phys. Rev. Lett.* **116**, 043201 (2016).
- [28] D. Primetzhofer, *Phys. Rev. A* **89**, 032711 (2014).
- [29] D. Roth, D. Goebel, D. Primetzhofer, and P. Bauer, *Nucl. Instrum. Methods Phys. Res., Sect. B* **317**, 61 (2013).
- [30] D. Goebel, W. Roessler, D. Roth, and P. Bauer, *Phys. Rev. A* **90**, 042706 (2014).
- [31] D. Primetzhofer, S. Rund, D. Roth, D. Goebel, and P. Bauer, *Phys. Rev. Lett.* **107**, 163201 (2011).
- [32] S. N. Markin, D. Primetzhofer, and P. Bauer, *Phys. Rev. Lett.* **103**, 113201 (2009).
- [33] T. T. Tran, L. Jablonka, B. Bruckner, S. Rund, D. Roth, M. A. Sortica, P. Bauer, Z. Zhang, and D. Primetzhofer, *Phys. Rev. A* **100**, 032705 (2019).
- [34] E. Runge and E. K. U. Gross, *Phys. Rev. Lett.* **52**, 997 (1984).
- [35] E. Fermi and E. Teller, *Phys. Rev.* **72**, 399 (1947).
- [36] E. A. Figueroa, E. D. Cantero, J. C. Eckardt, G. H. Lantschner, J. E. Valdés, and N. R. Arista, *Phys. Rev. A* **75**, 010901(R) (2007).
- [37] L. N. Serkovic Loli, E. A. Sánchez, O. Grizzi, and N. R. Arista, *Phys. Rev. A* **81**, 022902 (2010).
- [38] C. Archubi and N. Arista, *Eur. Phys. J. B* **89**, 86 (2016).
- [39] F. Mao, C. Zhang, J. Dai, and F.-S. Zhang, *Phys. Rev. A* **89**, 022707 (2014).
- [40] R. Ullah, F. Corsetti, D. Sánchez-Portal, and E. Artacho, *Phys. Rev. B* **91**, 125203 (2015).
- [41] J. Ziegler, J. Biersack, M. Ziegler, D. Marwick, and G. Cuomo, SRIM code, 2013, available from <http://srim.org>.
- [42] J. F. Ziegler, J. Biersack, and U. Littmark, *The Stopping and Range of Ions in Solids*, Vol. 1 (Springer, New York, 1985).
- [43] D. Marx and J. Hutter, *Ab Initio Molecular Dynamics: Basic Theory and Advanced Methods* (Cambridge University Press, Cambridge, England, 2009).
- [44] J. le Page, D. Mason, and W. Foulkes, *J. Phys.: Condens. Matter* **20**, 125212 (2008).
- [45] A. Caro, A. A. Correa, A. Tamm, G. D. Samolyuk, and G. M. Stocks, *Phys. Rev. B* **92**, 144309 (2015).
- [46] X. Li, J. C. Tully, H. B. Schlegel, and M. J. Frisch, *J. Chem. Phys.* **123**, 084106 (2005).
- [47] X. Andrade, A. Castro, D. Zueco, J. Alonso, P. Echenique, F. Falceto, and A. Rubio, *J. Chem. Theory Comput.* **5**, 728 (2009).
- [48] A. P. Horsfield, D. Bowler, A. Fisher, T. N. Todorov, and M. Montgomery, *J. Phys.: Condens. Matter* **16**, 3609 (2004).
- [49] F. Mao, C. Zhang, C.-Z. Gao, J. Dai, and F.-S. Zhang, *J. Phys.: Condens. Matter* **26**, 085402 (2014).
- [50] A. Castro, M. Isla, J. I. Martínez, and J. A. Alonso, *Chem. Phys.* **399**, 130 (2012).
- [51] J. L. Alonso, X. Andrade, P. Echenique, F. Falceto, D. Prada-Gracia, and A. Rubio, *Phys. Rev. Lett.* **101**, 096403 (2008).
- [52] X. Andrade, J. Alberdi-Rodríguez, D. A. Strubbe, M. J. Oliveira, F. Nogueira, A. Castro, J. Muguerza, A. Arruabarrena, S. G. Louie, A. Aspuru-Guzik, A. Rubio, and M. A. L. Marques, *J. Phys.: Condens. Matter* **24**, 233202 (2012).
- [53] M. A. Marques, M. J. Oliveira, and T. Burnus, *Comput. Phys. Commun.* **183**, 2272 (2012).
- [54] J. P. Perdew and Y. Wang, *Phys. Rev. B* **45**, 13244 (1992).

- [55] V. U. Nazarov, J. M. Pitarke, C. S. Kim, and Y. Takada, *Phys. Rev. B* **71**, 121106(R) (2005).
- [56] V. U. Nazarov, J. M. Pitarke, Y. Takada, G. Vignale, and Y.-C. Chang, *Phys. Rev. B* **76**, 205103 (2007).
- [57] N. Troullier and J. L. Martins, *Phys. Rev. B* **43**, 1993 (1991).
- [58] A. Castro, M. A. Marques, and A. Rubio, *J. Chem. Phys.* **121**, 3425 (2004).
- [59] M. Beekman, J. A. Kaduk, Q. Huang, W. Wong-Ng, Z. Yang, D. Wang, and G. S. Nolas, *Chem. Commun.* **8**, 837 (2007).
- [60] A. A. Correa, J. Kohanoff, E. Artacho, D. Sánchez-Portal, and A. Caro, *Phys. Rev. Lett.* **108**, 213201 (2012).
- [61] A. Schleife, Y. Kanai, and A. A. Correa, *Phys. Rev. B* **91**, 014306 (2015).
- [62] M. Caro, A. Correa, E. Artacho, and A. Caro, *Sci. Rep.* **7**, 2618 (2017).
- [63] A. V. Korol, V. G. Bezchastnov, G. B. Sushko, and A. V. Solov'yov, *Nucl. Instrum. Methods Phys. Res., Sect. B* **387**, 41 (2016).
- [64] N. P. Wang and I. Nagy, *Phys. Rev. A* **56**, 4795 (1997).
- [65] N. P. Wang, I. Nagy, and P. M. Echenique, *Phys. Rev. B* **58**, 2357 (1998).
- [66] D. Primetzhofer, *Phys. Rev. B* **86**, 094102 (2012).
- [67] T. Burnus, M. A. L. Marques, and E. K. U. Gross, *Phys. Rev. A* **71**, 010501(R) (2005).
- [68] R. Hatcher, M. Beck, A. Tackett, and S. T. Pantelides, *Phys. Rev. Lett.* **100**, 103201 (2008).
- [69] G. D. M. Azevedo, P. Grande, and G. Schiwietz, *Nucl. Instrum. Methods Phys. Res., Sect. B* **164**, 203 (2000).